Novel CV for Phase Transformation Electrodes

Yujie Zhu and Chunsheng Wang*

Department of Chemical & Biomolecular Engineering, University of Maryland, College Park, Maryland 20742, United States

Received: October 17, 2010; Revised Manuscript Received: November 24, 2010

Phase transformation cyclic voltammetry (CV) was developed by integrating mixed-control phase transformation theory and charge transfer effect with traditional CV model. This mixed-control phase transformation CV model was validated by good agreement between experimental CV data and simulated values from phase transformation CV for $LiFePO_4$. The lithium ion diffusion coefficient (10^{-16} m^2 s^{-1}) of $LiFePO_4$ obtained from the phase transformation CV model was 2 orders of magnitude higher than apparent values (10^{-18} m^2 s^{-1}) determined from traditional CV. The low diffusion coefficient from traditional CV is attributed to the disregard of phase transformation. In addition to the lithium ion diffusion coefficient, the interface mobility (on the magnitude of 10^{-14} m mol J^{-1} s^{-1}) of the $LiFePO_4$ electrode, which cannot be measured from traditional CV, was obtained using phase transformation CV. Using the phase transformation CV model, the CV curves of $LiFePO_4$ and $LiMnPO_4$ phase transformation electrodes were characterized, and the effects of lithium ion diffusion coefficient, interface mobility, exchange current density, and particle size on the CV profiles of phase transformation electrodes were systemically investigated.

1. Introduction

Recently, lithium ion (Li ion) batteries have received much attention for their potential applications in electric vehicles (EVs), hybrid electric vehicles (HEVs), and renewable energy storage.[1] Among all the electrode materials used in Li ion batteries, phase transformation materials (such as $LiFePO_4$, $Li_4Ti_5O_{12}$) are the most promising candidates due to their superior power density when compared to traditional solid solution material.[2−4] However, the mechanism of the exceptional rate performance of these phase transformation electrodes is still under debate due to the lack of reliable electroanalytical techniques suitable for phase transformation electrodes. All the traditional electroanalytical techniques, including potentiostatic intermittent titration technique (PITT),[5] galvanostatic intermittent titration technique (GITT),[5] electrochemical impedance spectroscopy (EIS)[6] and cyclic voltammetry (CV),[7] can only be used to analyze solid solution electrodes. Thus, the use of these traditional electroanalytical techniques to analyze the kinetics of phase transformation electrodes has received considerable controversy.[8−11]

Among these traditional electrochemical methods, CV is one of the most commonly used techniques for electrode kinetics studies. Unlike the GITT/PITT method, no thermodynamic information is needed for calculating the apparent diffusion coefficient, and complicated model fitting is not necessary compared to EIS. In CV tests, the electrode working potential is linearly cycled over some potential range at certain rates while the resultant current is recorded as a function of time (potential). By analyzing the resultant current versus potential profiles, both kinetic and thermodynamic information can be obtained. For example, the diffusion coefficient (D) of the active ions in a solid solution electrode can be calculated according to the linear relationship between the peak current and the square root of the scan rate (υ) in eq 1:[7]

$$i_p = 0.4463\left(\frac{F^3}{RT}\right)^{1/2} n^{3/2} A D^{1/2} C_0^* \upsilon^{1/2} \quad (1)$$

where i_p is the peak current (amperes), F is Faraday's constant (C mol^{-1}), n is the number of electrons involved in the reaction (mol), A is the contact area between electrode and electrolyte (m^2), D is the diffusion coefficient of active ions (m^2 s^{-1}), C_0^* is the initial concentration of active ions (mol m^{-3}), υ is the scan rate (v s^{-1}), and R and T have their usual meanings. Besides the diffusion coefficient, the potential difference between the cathodic and anodic peak current is normally used to evaluate the reversibility of the reaction. Also, high peak current value, spiculate peak shape and small peak potential separation are usually indicators for fast kinetics.

Recently, CV has been extensively used to study phase transformation materials[10,12−16] as a complementary method for constant current charge/discharge tests.[17−20] Like GITT, PITT, and EIS, the analysis of CV data is based on Fick's diffusion law without consideration of phase transformation. Thus, there is controversy surrounding the application of CV to phase transformation electrodes. For example, some investigators have found that Li ion insertion into $LiFePO_4$ is quasi-reversible because peak current varied linearly with scan rates, and the potential separation between cathodic and anodic current peaks varied with scan rates,[14,16] while other researchers reported that the lithiation/delithiation of $LiFePO_4$ is reversible due to an observed linear relationship between the peak current and the square root of scan rate.[10,12,15] Also, the apparent Li ion diffusion coefficient in $LiFePO_4$ obtained from traditional CV scans varied widely from 10^{-15} to 10^{-13} cm^2 s^{-1}. Since recent researchers have demonstrated that phase transformation plays a critical role in the charge/discharge of phase transformation electrodes,[3,21,22] the above results may come from the effect of phase transformation.

In previous studies, we developed a mixed-control phase transformation model[23] and integrated it with GITT and PITT

* Corresponding author. Tel: 301-405-0352. Fax: 301-314-9126. E-mail: cswang@umd.edu.

10.1021/jp109954y
Published on Web 12/13/2010

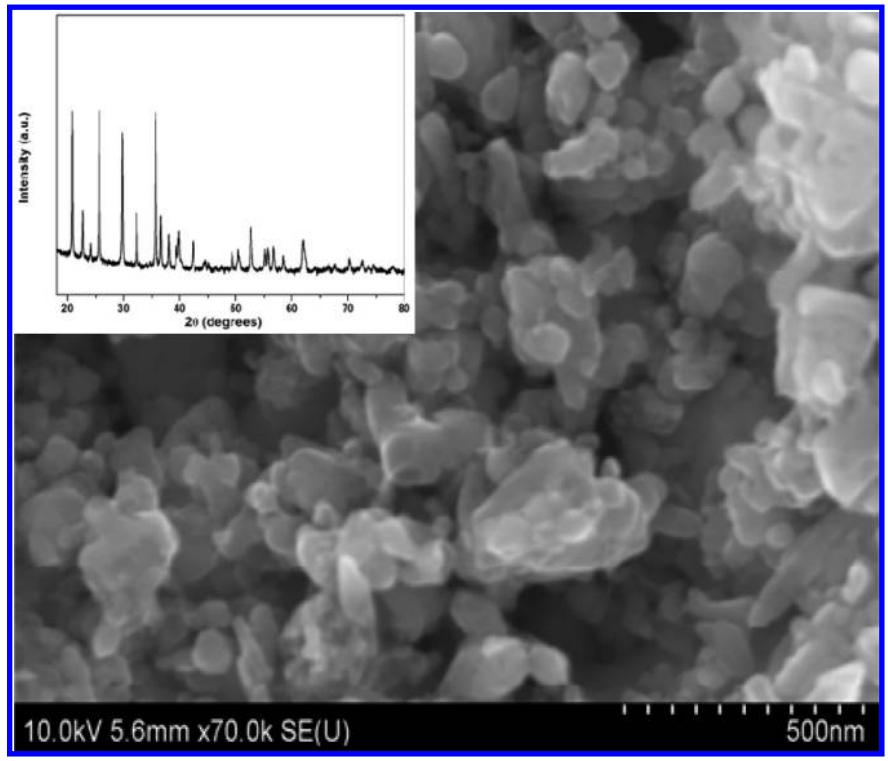

Figure 1. SEM image of the $LiFePO_4$ sample. The inset shows XRD patterns.

techniques to form phase transformation GITT and PITT.[24] For the first time, the Li ion diffusion coefficient and interface mobility of two $LiFePO_4$ samples in the two-phase region were obtained using phase transformation GITT.[24] In the present study, phase transformation CV is developed by integrating mixed-control phase transformation theory with traditional CV. In addition to ion diffusion and phase transformation, electrolyte resistance and charge transfer effect are also considered in phase transformation CV. In this study, the Li ion diffusion coefficient and interface mobility of $LiFePO_4$ were obtained by fitting the measured CV data with simulation results. These parameters were compared with values calculated from traditional CV theory. Also, the effect of phase transformation, ion diffusion coefficient, particle size, electrolyte resistance, and charge transfer resistance on the CV profiles was analyzed with the phase transformation CV model, and confirmed by the experimental CV curves of $LiFePO_4$ and $LiMnPO_4$ and the reported results in the literature.

2. Experiments

The carbon-coated $LiFePO_4$ powder was purchased from a commercial supplier. As shown in the SEM picture in Figure 1, the $LiFePO_4$ sample mainly consists of aggregations of small particles (300 nm) with a secondary particle size around 50 nm. The X-ray diffraction (XRD) pattern of the $LiFePO_4$ sample, shown as the inset in Figure 1, demonstrates that the $LiFePO_4$ sample is in a crystalline single phase. The $LiMnPO_4$ sample, provided by Prof. Manthiram at University of Texas, Austin, shows a particle size similar to $LiFePO_4$.

Three-electrode pouch cells each consisting of a working cathode, a Li foil anode, a Li wire reference electrode, polypropylene (PP) microporous film separators, and 1.0 M $LiPF_6$ in EC−DEC−DMC−EMC (1:1:1:3 by volume) liquid electrolyte (Ferro Corporation) were used for electrochemical measurements. The cathodes were prepared using the slurry coating method. The active materials were mixed with 10 wt % carbon black and 8 wt % polyvinylidene fluoride (PVDF) in 1-methyl-2-pyrrolidinone (NMP) solvent to form a viscous paste, which was then mixed for 45 min with a planetary ball milling machine. The obtained paste was then coated onto carbon-coated aluminum foil and dried in a vacuum oven at 120 °C overnight. After the foil cooled down to room temperature, 2 cm × 2 cm electrodes with active material loadings of 2 mg/cm^2 were cut out as cathodes for pouch cell assembly.

Before any electrochemical tests, the electrode was activated with five charge/discharge cycles from 2.2 to 4.2 V with a 0.1*C* current. To obtain the equilibrium potential-composition isotherm, the GITT tests were performed using *Arbin* instrumentation by repeatedly applying a current (less than *0.05C)* for 1 h and then resting for 16 h. Potentials of 4.2 and 2.2 V were used as high and low cutoff potentials in the GITT tests. For the CV measurements, the pouch cells were charged/discharged at different scan rates, ranging from 0.01 mV s^{-1} to 1 mV s^{-1}, from potentials of 2.5 to 4.2 V. Before each CV test, the electrode was discharged to 2.5 V using 0.1*C* current and held at 2.5 V for 2 h. Electrochemical impedance spectroscopy (EIS), with frequency ranging from 10^{-3} to 10^6 Hz and 10 mV potential amplitude, was used to measure the exchange current density of cathodes at different discharge/charge states. The EIS measurement was performed after the electrode was charged or discharged to desired state of charge (SOC) or state of discharge (SOD) and then rest for 2 h. Both CV and EIS were performed using a Solartron 1287/1260.

3. Model Development

The phase transformation process of $LiFePO_4$ during Li ion insertion/extraction and the mixed-control phase transformation model were discussed in our previous work.[24] Briefly, the lithiation/delithiation process of $LiFePO_4$ is described below.

At the beginning of Li ion insertion (discharge), Li ions insert into the particle surface layer and diffuse into the interior of the electrode particles to form a solid solution phase α

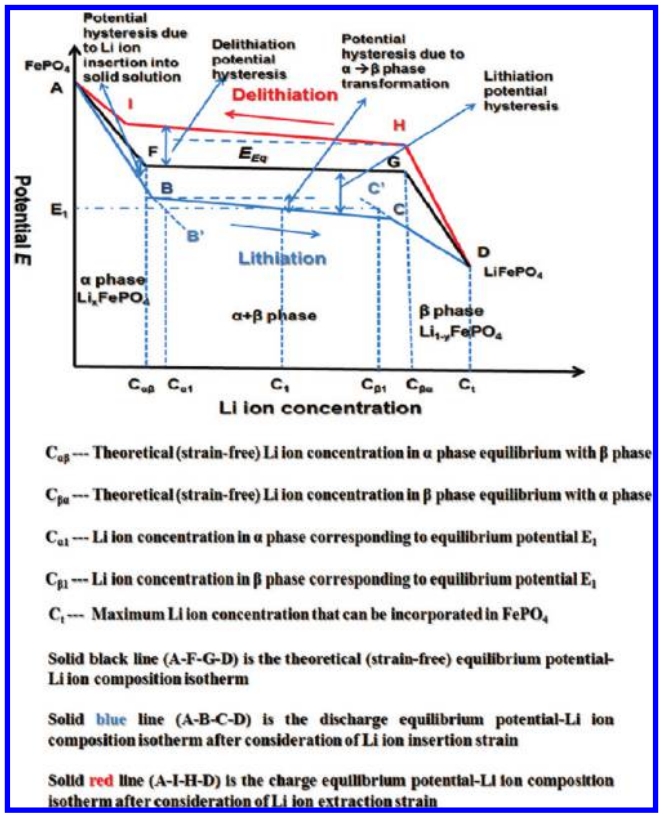

Figure 2. Schematic picture of charge/discharge processes for $LiFePO_4$.

(Li_xFePO_4). During the Li ion insertion, stress and strain are generated in the α phase, resulting in the lithiation potential drops below the theoretical (*strain-free*) equilibrium potential E_{eq} (A−F line). The actual discharge equilibrium potential E_{de} follows the line A−B in Figure 2 instead of the theoretical line A−F. When the Li ion insertion reaches point B in Figure 2, the β phase ($Li_{1-y}FePO_4$), with a different unit cell size from the α phase (Li_xFePO_4), will be formed. Due to the lattice misfit between the α and β phase, the growth of the β phase during Li ion insertion results in the accumulation of stress/strain, which gradually decreases the discharge equilibrium potential E_{de} (B−C line in Figure 2). During the phase transformation, the α phase coexists with the β phase while the equilibrium concentration of the α phase varies along the extension of the A−B line and the equilibrium concentration of the β phase follows the extension of the D−C line. For example, when the Li ion insertion level reaches C_1, the electrode has an equilibrium potential of E_1 (Figure 2) and is a mixture of α phase with composition $C_{\alpha 1}$ and β phase with composition $C_{\beta 1}$. When the electrode is dynamically discharged, the interfacial Li ion concentration is higher than the corresponding equilibrium concentration, and the concentration difference drives the phase transformation. However, the chemical potential of Li ion in the α phase at the sharp interface (*phase boundary between* α *and* β *phases*) is equal to the chemical potential of Li ion in the β phase at the interface, i.e. the dynamic interface Li ion concentration in the α and β phase always follows the extension of the A−B line and the D−C line at any time during the discharge process. Once the α phase completely transforms into the β phase, subsequent Li ion will start to dissolve into the β phase and form a solid solution with its maximum concentration as C_t (C−D line in Figure 2). Therefore, the lithiation equilibrium potential changes with Li ion composition (*capacity*) following the line A−B−C−D in Figure 2. A reverse phase transformation occurs during Li ion extraction but at a higher potential than that of Li ion insertion, following the line of D−H−I−A. The accommodation energy, which is due to the lattice misfit between two phases during phase transformation, leads to a potential hysteresis between lithiation and delithiation (Figure 2).

Phase transformation CV model was developed by integrating the mixed-control phase transformation theory with the traditional CV model with the consideration of both charge transfer resistance and electrode resistance (including electrolyte resistance and solid electrolyte interphase (SEI) resistance, etc). The details of phase transformation CV model can be found in the Supporting Information.

4. Results and Discussion

4.1. Parameter Determination for the Calculation of $LiFePO_4$ CV Profiles. ***Particle Size.*** As stated in ref 24, the characteristic length of a $LiFePO_4$ particle is the length of the aggregated particles, which is around 300 nm for the utilized $LiFePO_4$ sample (Figure 1).

Equilibrium Potential and Accommodation Energy. Figure 3a shows the plot of the equilibrium potential versus normalized capacity for $LiFePO_4$ obtained from the GITT test. The plateaus in Figure 3a correspond to the two-phase region, and the

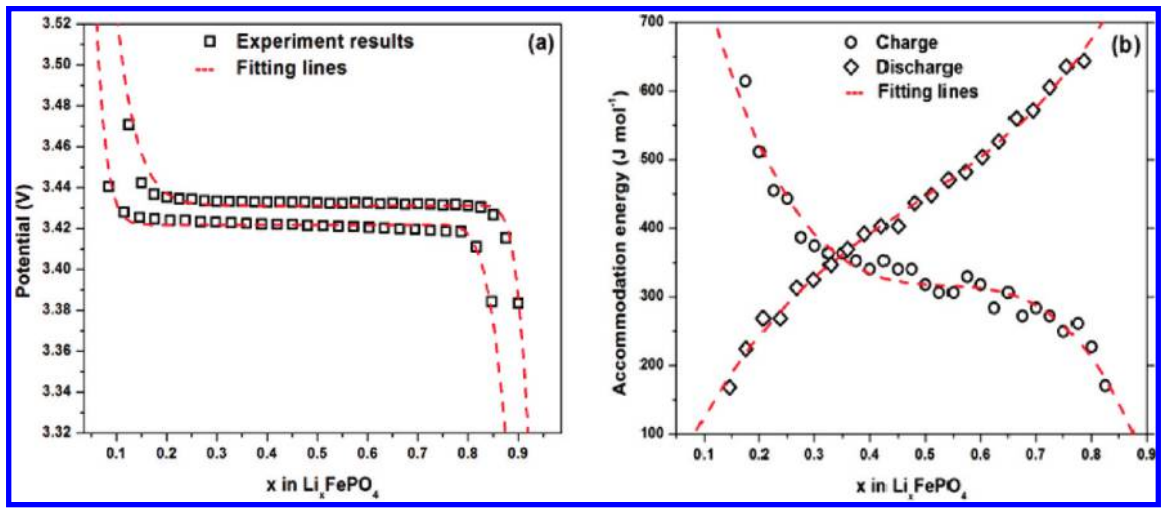

Figure 3. (a) Equilibrium potential−composition isotherm obtained from GITT, and (b) charge and discharge accommodation energy during phase transformation.

TABLE 1: Parameters Used for CV Simulations

parameters	charge	discharge
particle size (nm)	300	300
density of $FePO_4$ particle (ρ) (g/cm^3)	3.6	3.6
C_{max} (mol/cm^3)	0.02119	0.02119
strain-free equilibrium potential E_{eq} (V)	3.4279	3.4279
$\Delta G_{accom} = f(x_i)$ (J/mol)	$f(x_i) = 0.006113 - 0.01416x_i + 0.02510x_i^2 - 0.01510x_i^3$	$f(x_i) = 0.007197 - 0.007835x_i + 0.008458x_i^2 - 0.005820x_i^3$
equilibrium potential−composition isotherm for phase transformation $E(x)$	$E_c(x) = 3.43128 + 0.67858 \times \exp(-36.6886x^{1.27087}) - 2.1254\exp\left(-\frac{1.02622}{x^{12.56987}}\right)$	$E_d(x) = 3.4219 + 0.69926 \times \exp(-140.28201x^{1.52179}) - 2.16183\exp\left(-\frac{1.06065}{x^{7.86426}}\right)$
equilibrium potential−composition isotherm for α phase	$E_{\alpha c}(x_\alpha) = 2.7082 - 0.4301\ln\left(\frac{x}{1-x} + 0.03782\right)$	$E_{\alpha d}(x_\alpha) = 2.0311 - 0.6648\ln\left(\frac{x}{1-x} + 0.4296\right)$
equilibrium potential−composition isotherm for β phase	$E_{\beta c}(x_\beta) = 4.0760 - 0.3200\ln\left(\frac{x}{1-x} - 0.4613\right)$	$E_{\beta d}(x_\beta) = 3.8537 - 0.2884\ln\left(\frac{x}{1-x} - 0.1123\right)$
exchange current density i_0 for β phase ($A\ g^{-1}$)	0.25	0.32
exchange current density $i_0$for α phase ($A\ g^{-1}$)	0.4	0.54
electrode resistance (Ω) (including both SEI film and electrolyte resistance)	33	33
transfer coefficient γ	0.5	0.5

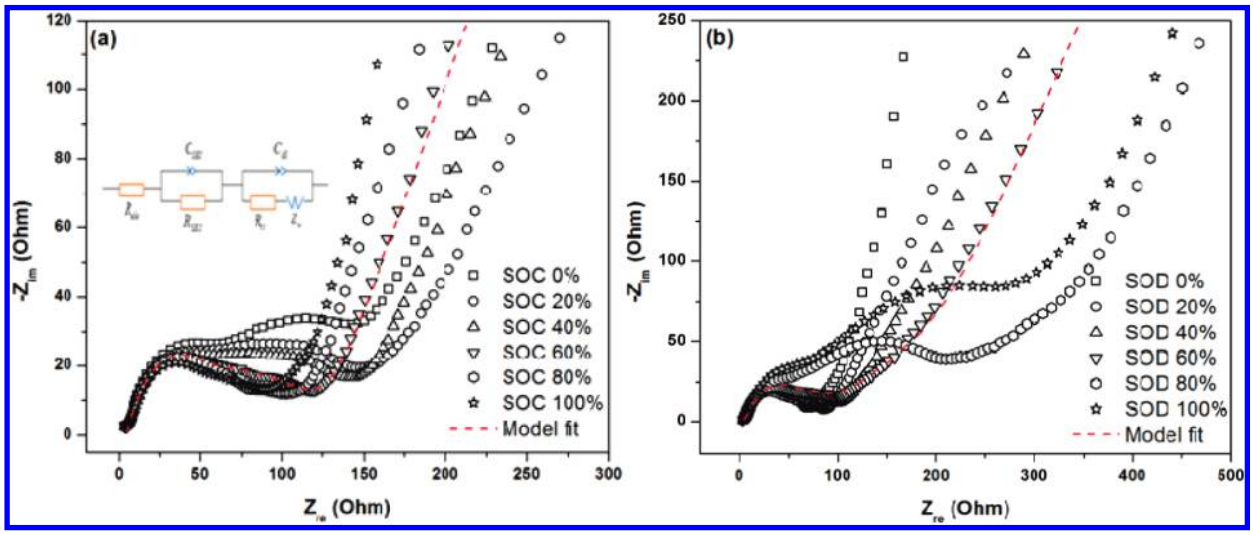

Figure 4. Electrochemical impedance spectroscopes of $LiFePO_4$ at different state of charge (a) and different state of discharge (b). The red dashed lines in both figures are fitting curves using the equivalent circuit inserted in (a). The equivalent circuit consists of a resistor, a resistor paralleled with a constant phase element (CPE), and a CPE parallel with a resistor which is connected with a Warburg element in series.

descending curves correspond to the single-phase region. Functions were fit to the equilibrium potential−composition isotherms (Table 1), and the resultant fitting lines (dashed lines in Figure 3a) well described the experimental data. The phase transformation accommodation energies during the charge and discharge process were calculated from the plot of equilibrium potential versus composition (Figure 3a) using eq S18 in the Supporting Information. The calculated phase transformation accommodation energy during charge and discharge are plotted in Figure 3b, and the relationship between the accommodation energy and the interface position (*ratio of transformed volume to total volume*) was expressed in Table 1 for both the charge and discharge processes. The theoretical (*strain-free*) equilibrium potential E_{eq} in the two-phase region, which was used to calculate the accommodation energy in eq S18 in the Supporting Information is determined by averaging the initial equilibrium phase transformation potentials during charge and discharge. As shown in Figure 3b, the discharge accommodation energy is larger than the charge accommodation energy at 50% SOD. The equilibrium potential−composition curves and accommodation energies of $LiFePO_4$ during lithiation and delithiation are similar to the results in our previous GITT study, although the two $LiFePO_4$ samples are provided by different vendors.[21]

Exchange Current Density and Electrode Resistance. To obtain the exchange current density i_0, the electrolyte resistance R_{ele}, and the SEI film resistance R_{SEI}, EIS tests were performed on $LiFePO_4$ electrodes at different SOD and SOC. Figure 4a and Figure 4b show the Nyquist plot of the $LiFePO_4$ electrode at different charge and discharge states. The Nyquist plots of the $LiFePO_4$ electrode consist of two semicircles at high and middle frequency and a straight line at low frequency. The high frequency semicircle is attributed to the SEI film, the middle

TABLE 2: Charge Transfer Resistance and Exchange Current Density at Different State of Discharge (SOD) and State of Charge (SOC)

	charge		discharge	
SOD/(SOC)	R_{ct} (Ω)	i_0 (A g^{-1})	R_{ct} (Ω)	i_0 (A g^{-1})
0%/(100%)	103.3	0.248	158.1	0.16
20%/(80%)	90.42	0.281	134.3	0.19
40%/(60%)	95.8	0.296	63.68	0.4
60%/(40%)	71.29	0.356	60.8	0.42
80%/(20%)	61.21	0.420	54.0	0.47
100%/(0%)	60.86	0.422	47.1	0.54

frequency semicircle to the charge transfer, and the low frequency line to the Li ion diffusion. As shown in Figure 4a and Figure 4b, both the SEI film resistance and the charge transfer resistance slightly increase with the SOD and decrease with the SOC, but the electrolyte resistance remains stable. The charge transfer, SEI film, and electrolyte resistance at different SOC and SOD were obtained by fitting the impedance data with the equivalent circuit (inset in Figure 4a). The combined electrolyte resistance and SEI film resistance are defined as the electrode resistance in this study. The exchange current was calculated from the charge transfer resistance R_{ct} according to following equation:

$$i_0 = \frac{RT}{FR_{ct}} \tag{2}$$

where R is the universal gas constant (J mol^{-1} K^{-1}), T is the temperature (K), F is Faraday constant (C mol^{-1}) and R_{ct} is the charge transfer resistance (Ω). The charge transfer resistances and corresponding exchange current density measured at different SOC and SOD were listed in Table 2.

During the discharge process of a fully charged $LiFePO_4$ electrode, the outer phase in contact with the electrolyte changes from the initial Li ion deficient phase (α phase) to the Li ion rich phase (β phase) when phase transformation starts. Since the charge transfer reaction occurs on the surface of $LiFePO_4$ particles in contact with the electrolyte, the exchange current of α phase was determined from EIS at 0% SOD (Table 2) and the exchange current of β phase was obtained by averaging the exchange currents measured from EIS at SOD of 20%, 40%, 60%, 80% and 100% (Table 2). The exchange currents of α and β phases are listed in Table 1. Similarly, the average values of the exchange current of the initial β phase and the following α phase in the charge process were also calculated and are listed in Table 1. Since the double layer capacitance and SEI layer capacitance are small, and the scan rates in CV are low, SEI film impedance is treated as pure resistance.

The development of the phase transformation cyclic voltammtery model is discussed in the Supporting Information. By numerically solving the differential equations under corresponding initial and boundary conditions with the numerical method of lines (MOL) approach in the Maple software,[24] the Li ion concentration profiles and the current densities during the CV process can be obtained. Since the particle size, equilibrium potential, accommodation energy, exchange current density, and electrode resistance in the phase transformation CV equations are determined, unknown parameters are only diffusion coefficients and interface mobility which can be obtained by curve fitting between experimental CV data and simulated results from the mixed-control model through adjusting these parameters.

4.2. Validation of Phase Transformation CV and Comparison with Traditional CV. Figure 5 shows the experimental and simulated CV curves of $LiFePO_4$ at different scan rates. As shown in Figure 5, the charge and discharge CV scans consist of anodic and cathodic current peaks corresponding to the Fe^{2+}/Fe^{3+} redox couple. Both the peak current values and peak potential separations increase with the scan rates, which is in agreement with results reported by other researchers.[13−16] The experimental CV were fitted using phase transformation CV model with determined parameters (exchange current, electrode resistance, particle size, equilibrium potential and accommodation energy) and three adjustable parameters (diffusion coefficients in α (D_α) and β (D_α) phases and the interface mobility). As presented in Figure 5, the good agreement between the experimental data and simulation results at various scan rates validates the mixed-control CV model.

Figure 6 shows the relationship between peak current and square root of scan rate obtained from the experimental data in Figure 5. As shown in Figure 6, the anodic (delithiation) and cathodic (lithiation) peak currents both show linear dependence on the square root of the scan rate at the scan rates under 0.2 mV s^{-1}. However, when the scan rate is higher than 0.2 mV s^{-1}, the peak currents are smaller than the values predicted by the traditional CV theory (dashed line in Figure 6). This observation is in agreement with results reported by other researchers.[14] This deviation from a linear relationship suggests that $LiFePO_4$ may not be solely controlled by Li ion diffusion, and that phase transformation needs to be considered.

According to Figure 6, the diffusion coefficients for both the anodic and cathodic processes were calculated based on the traditional CV theory using eq 1, and the obtained values were presented in Figure 7a as dashed lines. As shown in Figure 7a, the diffusion coefficient calculated from eq 1 using traditional CV theory is on the order of $10^{-19}-10^{-18}$ m^2 s^{-1}, which agrees with the value obtained by other researchers using traditional CV[14,15] and traditional EIS in a two-phase region.[10] However, the obtained diffusion coefficients from traditional CV are 1 or 2 orders of magnitude lower than those measured in the single-phase region using traditional GITT[24] and PITT.[10] This result is unreasonable since the composition and structure of the α phase before and after β phase deposition are almost the same, so the diffusion coefficient of Li ion in the α phase should be similar before and after β phase formation. The reduced diffusion coefficient using traditional (single phase) CV may be attributed to a slow phase transformation, which is neglected in traditional CV.

Using comprehensive phase transformation CV, the Li ion diffusion coefficient and interface mobility for both the anodic and cathodic processes were obtained by curve fitting and plotted in Figure 7a and Figure 7b. The current density is directly related to the Li ion flux on the surface of outer phase which directly contacts electrolyte. In the phase transformation region, the outer phase is α phase and the inner phase is β phase during the charge process, while the inner phase is α phase and the outer phase is β phase during discharge process. Our simulations appropriately found that the Li ion diffusion coefficient of the inner phase had a minor effect on the resultant CV profiles when compared to the outer phase. So, only the Li ion diffusion coefficients for the outer phase, e.g. D_α for the anodic (charge) and D_β for the cathodic (discharge) process, were plotted against scan rate in Figure 7a. The diffusion coefficient obtained through curve fitting by phase transformation CV is on the order of 10^{-16} m^2 s^{-1}, which is 2 or 3 orders higher than the value calculated from eq 1 using traditional CV, but is close to the values in the single

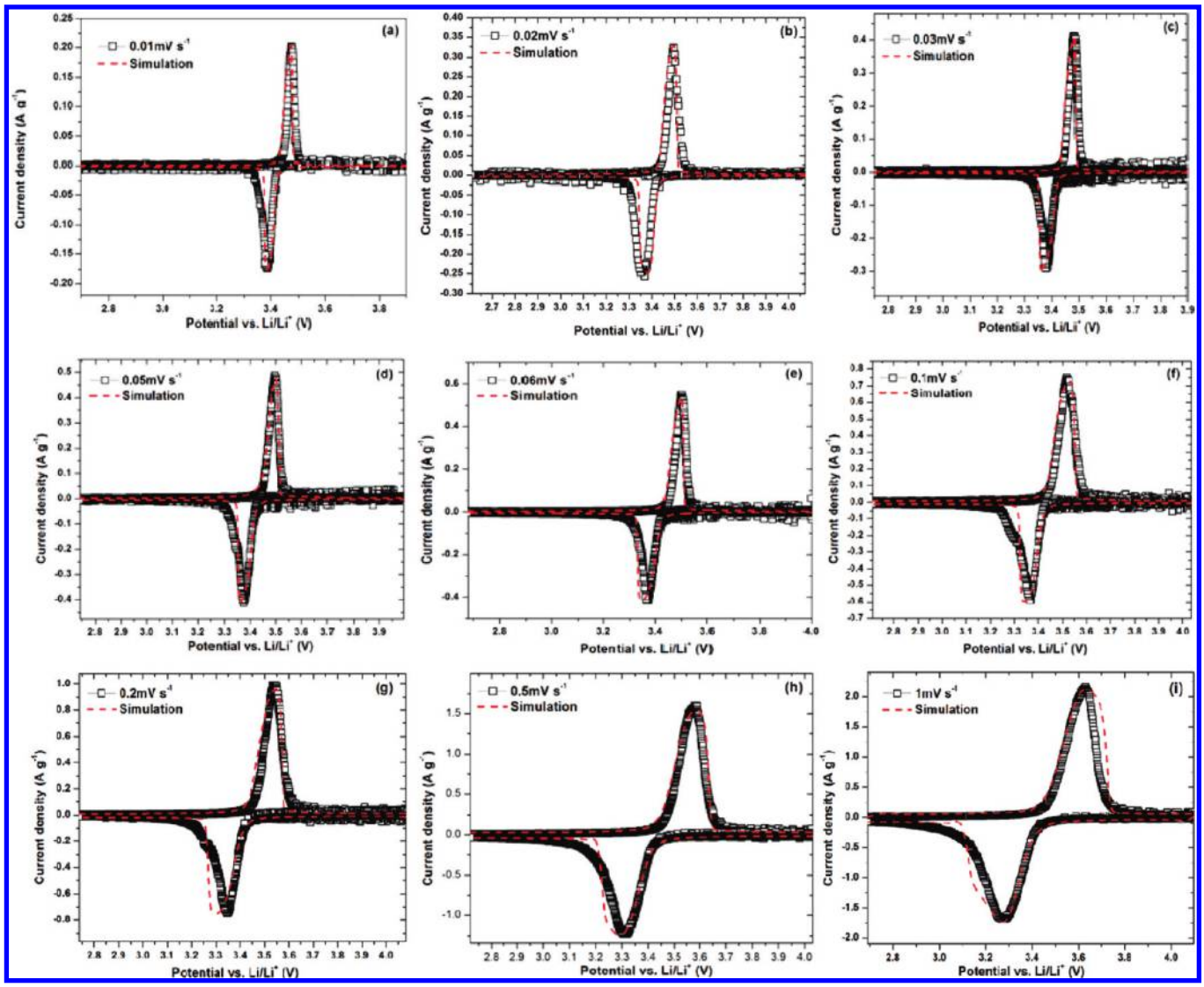

Figure 5. Comparison between measured CV profiles and simulated CV curves at different scan rates: (a) 0.01 mV s^{-1}, (b) 0.02 mV s^{-1}, (c) 0.03 mV s^{-1}, (d) 0.05 mV s^{-1}, (e) 0.06 mV s^{-1}, (f) 0.1 mV s^{-1}, (g) 0.2 mV s^{-1}, (h) 0.5 mV s^{-1}, (i) 1 mV s^{-1} (symbols, experiments; dashed lines, model).

α or β phase region obtained through GITT,[24] PITT[10] and EIS.[10] Therefore, phase transformation CV can accurately determine the diffusion coefficient of phase transformation electrodes at the phase transformation region. The interface mobility obtained from phase transformation CV is plotted against scan rate in Figure 7b, which is on the order of 10^{-14} m mol J^{-1} s^{-1}. Both the Li ion diffusion coefficient (Figure 7a) and the interface mobility (Figure 7b) obtained through phase transformation CV in this study are slightly higher than previously obtained values using phase transformation GITT.[24] Two possible reasons are (1) the disregard of the charge transfer and SEI/electrolyte resistance in phase transformation GITT, and (2) the use of different $LiFePO_4$ samples in the two studies. It has been demonstrated that, without consideration of electrode resistance (charge transfer, SEI film and electrolyte), the obtained diffusion coefficient is lower than its real value.[25] Yu et al.[14] reported that the electrolyte compositions and electrode thickness also affect the peak current, suggesting that the electrode resistance and exchange current need to be included in the model. As shown in Figure 7a, the Li ion diffusion coefficient obtained by curve fitting is higher for the anodic process (D_α) than the cathodic process (D_β), which demonstrates that Li ion diffusion coefficient in Li_xFePO_4 is slightly higher than that in $Li_{1-y}FePO_4$,

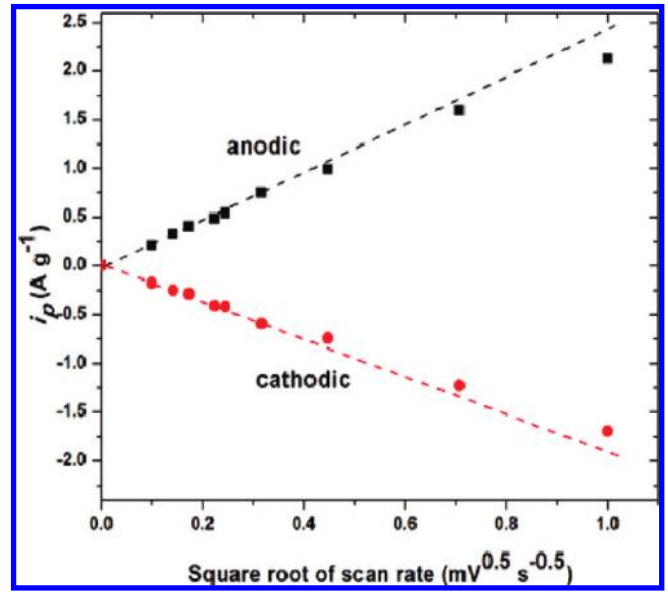

Figure 6. Dependence of peak currents of $LiFePO_4$ on square root of scan rate for $LiFePO_4$ sample.

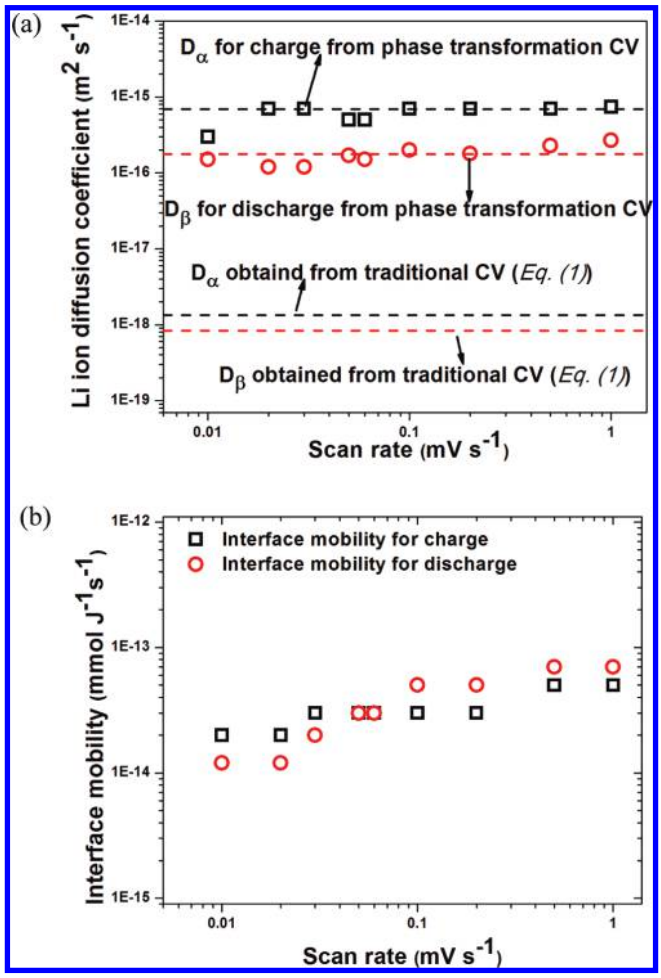

Figure 7. (a) Li ion diffusion coefficient and (b) interface mobility in $LiFePO_4$ obtained by curve fitting from phase transformation CV.

although the interface mobility is on the same order in Figure 7b. The higher diffusion constant on the charge (oxidation) reaction than that obtained in the discharge (reduction) process of $LiFe_xMn_{1-x}PO_4$ at any Mn^{2+} substitution degree was also reported by Nakamura.[15] This might be one of the reasons why the charge rate capability is better than the discharge rate capability for $LiFePO_4$.[26]

To investigate the role of phase transformation (Figure 6), CV profiles of $LiFePO_4$ at different scan rates were simulated with various interface mobility values. The resultant anodic peak current (i_p) was plotted against the square root of the scan rate ($v^{0.5}$) in Figure 8. As shown in Figure 8, when the interface mobility is 10^{-11} m mol J^{-1} s^{-1} or larger, which is much higher than the typical value of 10^{-14} m mol J^{-1} s^{-1} for current $LiFePO_4$, i_p shows a linear dependence on $v^{0.5}$ in entire scan rate. In this case, the Li ion diffusion controls the CV scan, and the relationship between the peak currents and scan rates obeys traditional diffusion-controlled CV theory. When the interface mobility is 10^{-14} m mol J^{-1} s^{-1} (a value for current $LiFePO_4$ sample), the process is supposed to be controlled by both ion diffusion and phase transformation, and i_p is linearly related to $v^{0.5}$ under a scan rate of 0.1 mV s^{-1} and then deviates negatively from the straight line at higher scan rates, which is similar to the curve in Figure 6. When the interface mobility decreases to 10^{-17} m mol J^{-1} s^{-1}, the phase transformation rate is too slow, and the anodic process is supposed to be under phase transformation control; i_p only shows a linear dependence on $v^{0.5}$ under a scan rate of 0.08 mV s^{-1}, with the following scan rates showing a positive deviation from the initial straight line. This result suggests that phase transformation has a significant effect on the resultant i_p vs $v^{0.5}$ curve for CV. When we calculate the apparent diffusion coefficient by using the plot of i_p vs $v^{0.5}$, the effect of phase transformation has to be considered.

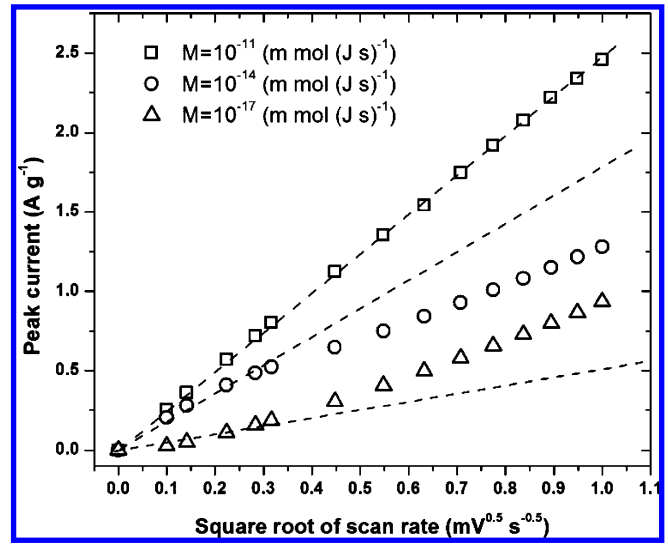

Figure 8. Simulated dependence of peak current of $LiFePO_4$ on square root of scan rate at constant diffusion coefficients ($D_\alpha = 5 \times 10^{-16}$ m^2 s^{-1} and $D_\beta = 2 \times 10^{-16}$ m^2 s^{-1}) but different interface mobilities.

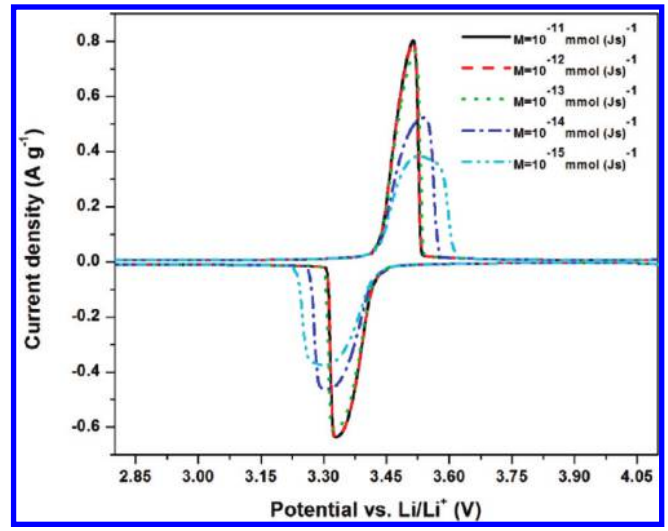

Figure 9. Simulated CV profiles of $LiFePO_4$ at different interface mobility values (scan rate 0.1 mV s^{-1}; $D_\alpha = 5 \times 10^{-16}$ m^2 s^{-1} and $D_\beta = 2 \times 10^{-16}$ m^2 s^{-1}).

4.3. Characterization of Phase Transformation Electrodes Using the Phase Transformation CV Technique. To realize the power of the CV technique in the characterization of phase transformation electrodes, the CV profiles of phase transformation electrodes should be analyzed using phase transformation CV. Therefore, the effects of phase transformation, electrode resistance, and ion diffusion on the CV profiles are all accounted for.

Effect of Phase Transformation on CV Profiles. Figure 9 presents simulated phase transformation CV profiles at a scan rate of 0.1 mV s^{-1} with interface mobility values ranging from 10^{-15} to 10^{-11} m mol J^{-1} s^{-1}. As shown in Figure 9, both the anodic and cathodic peak currents increase as the interface mobility increases. No significant difference exists between CV profiles when interface mobility is larger than 10^{-12} m mol J^{-1} s^{-1}. As the interface mobility increases, the peak current profile

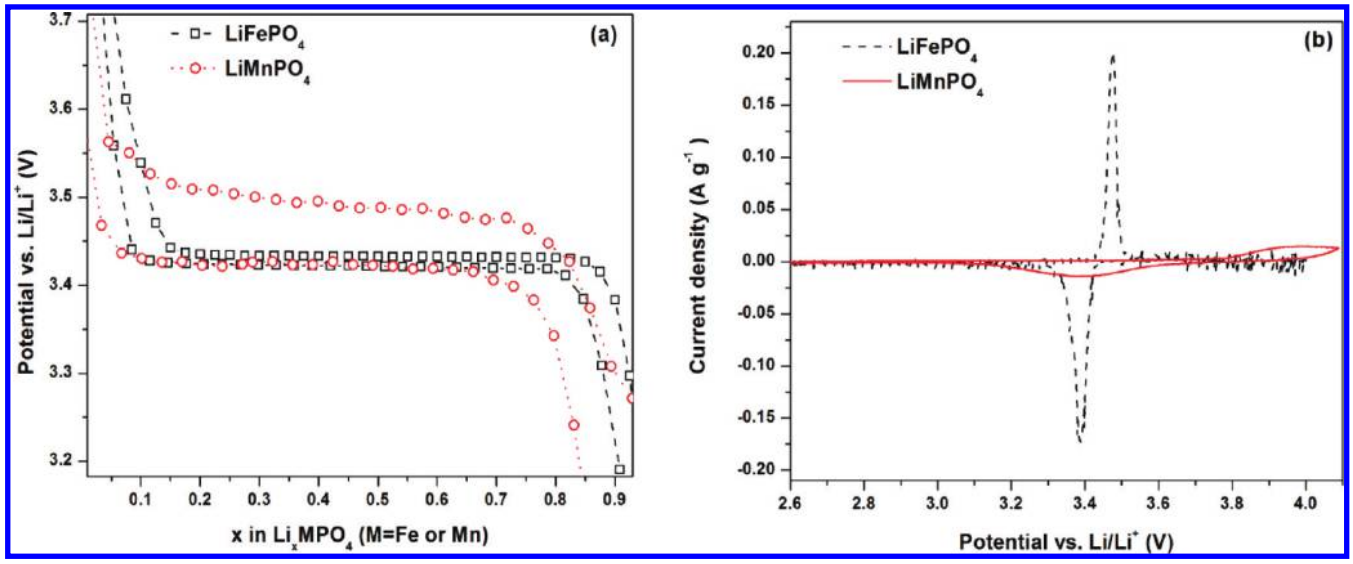

Figure 10. (a) Equilibrium potential−composition isotherm of $LiFePO_4$ and $LiMnPO_4$ electrodes measured using GITT, (b) measured CV curves of $LiFePO_4$ and $LiMnPO_4$ at scan rate 0.01 mV s^{-1}. (To better compare both GITT and CV results between $LiFePO_4$ and $LiMnPO_4$, the Li insertion potentials of $LiMnPO_4$ were shifted to the same lithiation potential of $LiFePO_4$.)

becomes sharp, and the potential separation between the anodic and the cathodic peak currents becomes narrow.

The effect of interface mobility on CV curves in Figure 9 was confirmed by the difference of CV profiles between $LiFePO_4$ and $LiMnPO_4$ in Figure 10b. As $LiFePO_4$, $LiMnPO_4$ also undergoes a first order phase transformation during charge and discharge but at a higher redox potential of 4.1 V, which makes it a promising candidate for cathode materials of Li ion batteries. To easily compare two CV curves, the discharge equilibrium potential (4.1 V) of $LiMnPO_4$ is shifted to the discharge equilibrium potential (3.4 V) of $LiFePO_4$ (Figure 10). Unlike $LiFePO_4$, $LiMnPO_4$ has much lower interface mobility than that of $LiFePO_4$ due to a large volume change during phase transformation.[3,27,28] The large volume change in $LiMnPO_4$ also enhances the strain accommodation energy in phase transformation, resulting in a larger potential hysteresis in Figure 10a and wider potential separation between anodic and catholic peak currents in Figure 10b. Figure 10a shows a comparison of the equilibrium potential−composition isotherms between shifted $LiMnPO_4$ and $LiFePO_4$ measured by GITT. The potential hysteresis between the charge and discharge equilibrium potential is around 70 mV for $LiMnPO_4$, which is 7 times higher than that of $LiFePO_4$ (10 mV). Figure 10b shows the CV curves for both materials at a scan rate 0.01 mV s^{-1}. A slow scan rate was used because of the poor kinetics of $LiMnPO_4$. The $LiMnPO_4$ and $LiFePO_4$ samples tested in Figure 9 have a comparable particle size, and both were coated with carbon to increase the electronic conductivity. Compared to the $LiFePO_4$ CV curve, the CV curve for $LiMnPO_4$ has much smaller peak current values, a wider peak shape, and larger peak potential separation, which is in agreement with the simulated CV profile of phase transformation electrodes with low interface mobility (Figure 9). Therefore, if all other electrode properties are the same, the peak current value and peak shape can be used to roughly judge the relative value of the interface mobility between phase transformation electrodes. The peak potential separation can be used to evaluate both thermodynamic potential hysteresis and reaction kinetics, which will be shown below.

Effects of the Electrode Properties on the CV Profiles. Different electrode parameters have different effects on CV profiles. If we know how the electrode parameters affect the resultant CV profiles of phase transformation electrodes, we can analyze the thermodynamics and kinetics of the reaction by comparing phase transformation CV profiles.

The effect of the Li ion diffusion coefficient and the particle size on CV profiles was investigated. As shown in Figure 11, with the increasing of Li ion diffusion coefficient or decreasing of particle size, the peak currents increase and become sharp due to the improvement of Li ion transport. The potential separation between anodic and cathodic peak currents did not show a general increase or decrease as of the Li ion diffusion coefficient or sample particle size changed.

The diffusion coefficient mentioned above is a chemically effective diffusion coefficient that considers the movement of both the Li ion and electron, and can be obtained by following equation:[29]

$$D = \frac{2D_{Li^+}D_e}{D_{Li^+}D_e} \tag{3}$$

where D is the chemical diffusion coefficient, and D_{Li^+} and D_e are the diffusion coefficients for the Li ion and electron, which can be related to the ionic and electronic conductivity by the Nernst−Einstein equation.[30] Coating carbon or other conductive materials can greatly improve the electronic conductivity of the electrode materials, which also increases the chemical diffusion coefficient. The CV profiles of uncoated and carbon nanotube coated $LiFePO_4$ in ref 31 and the CV curves of uncoated and PbZe coated $LiFePO_4$ in ref 32 are very similar to the simulation results shown in Figure 11, validating the mixed-control phase transformation CV model.

Figure 12 demonstrates the effects of different electrode resistances on CV profiles. Figure 12a shows CV profiles for different charge transfer resistances with the exchange current density ranging from $0.01i_0$ to $100i_0$, where i_0 is the exchange current density measured for current $LiFePO_4$ sample. As shown in Figure 12a, with the increasing of the charge transfer resistance (decreasing of exchange current density), the peak currents of the CV profile decreased, the potential separation between the anodic and the cathodic peak current enlarged, and the peak current profiles became wide. In Figure 12b, as the electrode resistance R_e (includes the electrolyte and SEI film

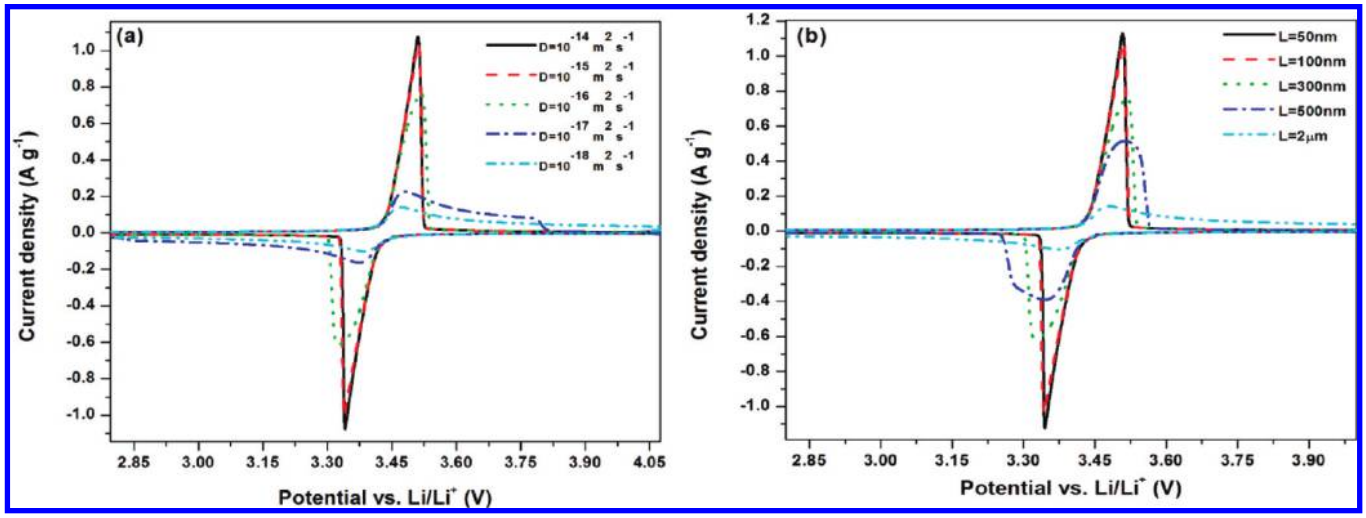

Figure 11. Simulated CV profiles of $LiFePO_4$ at (a) different Li ion diffusion coefficients, (b) different sample particle sizes with scan rate 0.1 mV s^{-1} (interface mobility $M = 10^{-13}$ m mol (J s)$^{-1}$, particle size in (a): $L = 300$ nm).

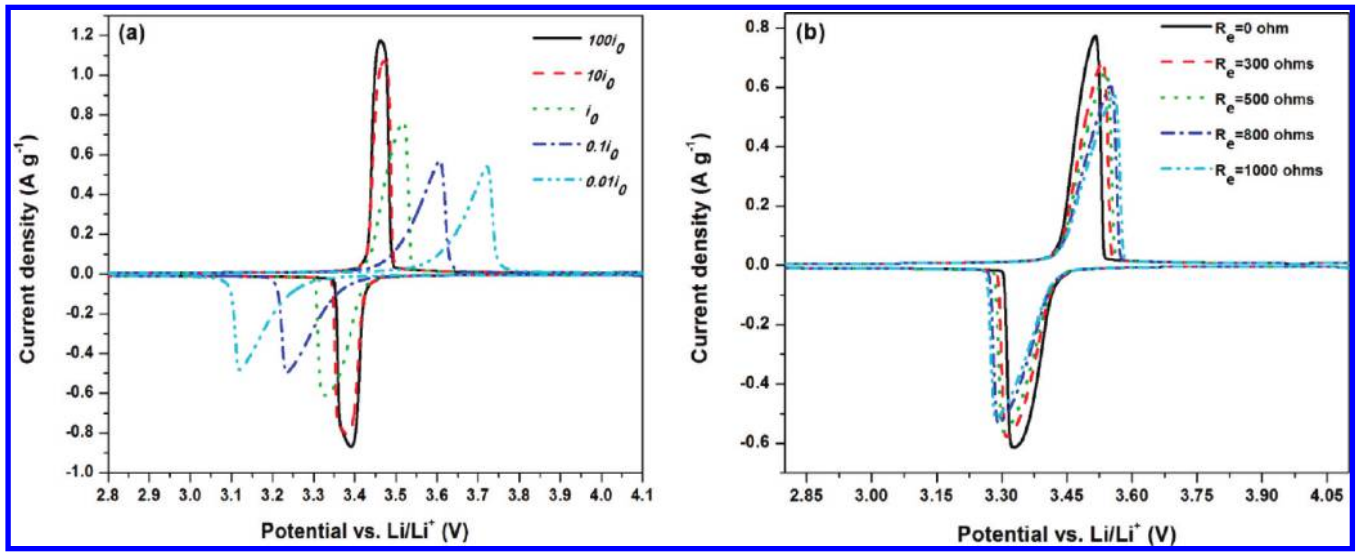

Figure 12. Simulated CV profiles at (a) different charge transfer resistances, (b) different electrode resistances (scan rate 0.1 mV s^{-1}; $D_\alpha = 5 \times 10^{-16}$ m^2 s^{-1}, $D_\beta = 2 \times 10^{-16}$ m^2 s^{-1} and $M = 10^{-13}$ m mol (J s)$^{-1}$).

resistance) increases from 0 to 1000 ohms, the changes in the CV profiles are analogous to the above-described changes in Figure 12a. The simulated CV profiles under different exchange current densities in Figure 12a were confirmed by the CV results of $LiFePO_4$ electrodes with different exchange currents (Figure 13). The different exchange currents for $LiFePO_4$ electrode were obtained using EIS after charging/discharging the electrode at 1*C* rate for different cycles. As shown in Figure 13, with the increasing of the charge transfer resistance (*decreasing of exchange current density*), the peak currents of the CV profiles decreased, the peak potential separation increased, and the peak shape became wider, which are the predicted trends from phase transformation CV. The CV profile of a $LiFePO_4$ electrode in different electrolytes reported by Yu et al.[14] is also similar to the simulated CV profile in Figure 12a. Since the charge transfer resistance of $LiFePO_4$ electrodes changes with electrolyte composition, the difference in CV profiles in ref 14 can be attributed to the difference in exchange current densities of $LiFePO_4$ in different electrolytes.

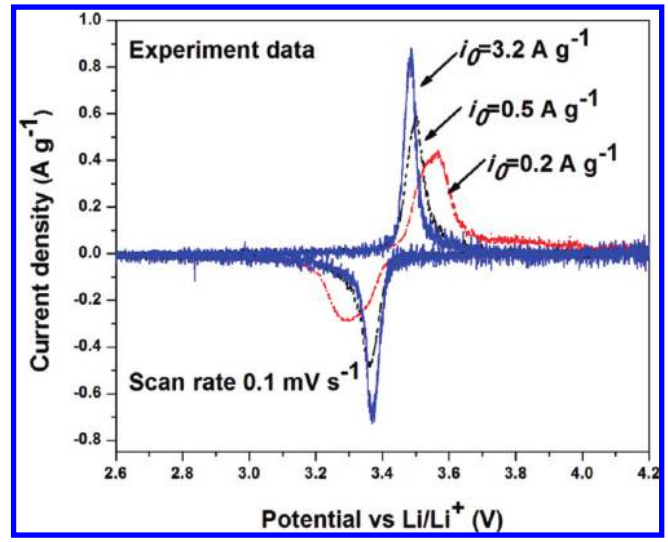

Figure 13. Measured CV curves of a $LiFePO_4$ electrode with different exchange currents.

5. Conclusions

Phase transformation cyclic voltammetry (CV) based on mixed-control phase transformation theory was developed in this study. $LiFePO_4$ is used as a specific example to validate this model. The agreement between the simulated CV profiles

and the experimental data at different scan rates validates this phase transformation CV model. The diffusion coefficient (10^{-16} m^2 s^{-1}) of $LiFePO_4$ obtained through curve fitting using phase transformation CV model is 2 or 3 orders of magnitude larger than that determined using traditional CV, which is due to the inclusion of phase transformation, charge transfer and electrode resistances in mixed-control model. The interface mobility (10^{-14} m mol J^{-1} s^{-1}) obtained by phase transformation CV is slightly higher than that obtained from phase transformation GITT,[24] since the charge transfer resistance and electrode resistance, which were not considered in phase transformation GITT, are included in this comprehensive phase transformation CV model.

Phase transformation CV is also a powerful technique for analyzing the thermodynamics and kinetics of phase transformation electrodes. The potential separation between peak currents in CV will provide relative values of the potential hysteresis or charge transfer resistance. The change in peak current and peak shape can be used to evaluate the interface mobility (M) and diffusion capability (L^2/D). Phase transformation CV demonstrated that the peak potential separation increased with increasing potential hysteresis and decreasing exchange current, which was confirmed through comparisons of CV profiles of $LiFePO_4$ and $LiMnPO_4$ electrodes and the profiles of the $LiFePO_4$ electrode at different charge/discharge cycles. Also, the peak current increases and peak shape becomes sharp with increasing interface mobility and diffusion capability, which is in agreement with reported CV profiles.

Acknowledgment. The authors gratefully acknowledge the support of the National Science Foundation under Contract No. CBET0933228 (Dr. Maria Burka, Program Director) and of the Army Research Office under STIR Contract No. W911NF0810441 (Dr. Robert Mantz, Program Manager). The authors also thank Prof. Manthiram at University of Texas, Austin, for the $LiMnPO_4$ cells and Dr. Xilin Chen for the SEM and XRD tests.

Supporting Information Available: Details of the phase transformation CV model. This material is available free of charge via the Internet at http://pubs.acs.org.

References and Notes

(1) Chalk, S. G.; Miller, J. F. *J. Power Sources* **2006**, *159*, 73.
(2) Chung, S. Y.; Bloking, J. T.; Chiang, Y. M. *Nat. Mater.* **2002**, *1*, 123.
(3) Meethong, N.; Huang, H. Y. S.; Speakman, S. A.; Carter, W. C.; Chiang, Y. M. *Adv. Funct. Mater.* **2007**, *17*, 1115.
(4) Funabiki, A.; Inaba, M.; Abe, T.; Ogumi, Z. *J. Electrochem. Soc.* **1999**, *146*, 2443.
(5) Wen, C. J.; Boukamp, B. A.; Huggins, R. A. *J. Electrochem. Soc.* **1979**, *126*, 2258.
(6) Ho, C.; Raistrick, I. D.; Huggins, R. A. *J. Electrochem. Soc.* **1980**, *127*, 345.
(7) Bard, A. J.; Faulkner, L. R. *Electrochemical Methods*, John Wiley & Sons, Inc.: New York, 1980.
(8) Levi, M. D.; Markevich, E.; Aburbach, D. *J. Phys. Chem. B* **2005**, *109*, 7420.
(9) Prosini, P. P.; Lisi, M.; Zane, D.; Pasquali, M. *Solid State Ionics* **2002**, *148*, 45–51.
(10) Xie, J.; Imanishi, N.; Zhang, T.; Hirano, A.; Takeda, Y.; Yamamoto, O. *Electrochim. Acta* **2009**, *54*, 4631.
(11) Rho, Y. H.; Kanamura, K. *J. Solid State Chem.* **2004**, *1771*, 2094–2100.
(12) Nakamura, T.; Sakumoto, K.; Seki, S.; Kobayashi, Y.; Tabuchi, M.; Yamada, Y. *J. Electrochem. Soc.* **2007**, *154*, A1118.
(13) Franger, S.; Bourbon, C.; Le Cras, F. *J. Electrochem. Soc.* **2004**, *151*, A1024.
(14) Yu, D. Y.; Fietzek, C.; Weydanz, W.; Donoue, K.; Inoue, T.; Kurokawa, H.; Fujitani, S. *J. Electrochem. Soc.* **2007**, *154*, A253.
(15) Nakamura, T.; Sakumoto, K.; Okamoto, M.; Seki, S.; Kobayashi, Y.; Takeuchi, T.; Tabuchi, M.; Yamada, Y. *J. Power Sources* **2007**, *174*, 435.
(16) Takahashi, M.; Tobishima, S.; Takei, K.; Sakurai, Y. *Solid State Ionics* **2002**, *148*, 283.
(17) Konarova, M.; Taniguchi, I. *Mater. Res. Bull.* **2008**, *43*, 3305.
(18) Ni, J. F.; Zhou, H. H.; Chen, J. T.; Zhang, X. X. *Mater. Lett.* **2005**, *59*, 2361.
(19) Liu, H.; Cao, Q.; Fu, L. J.; Li, C.; Wu, Y. P.; Wu, H. Q. *Electrochem. Commun.* **2006**, *8*, 1553.
(20) Ma, J.; Qin, Q. *J. Power Sources* **2005**, *148*, 66.
(21) Chiang, Y.-M.; Meethong, N.; Huang, H.-Y. S.; Carter, W. C.; Chang, S.; Hsiao, A.; Gozdz, A. S. ESC Meeting, Cancun, Mexico, November 2006.
(22) Meethong, N.; Huang, H.-Y. S.; Speekman, S. A.; Carter, W. C.; Chiang, Y.-M. *Electrochem. Solid-State Lett.* **2007**, *10*, A134.
(23) Wang, C.; Kasavajjula, U.; Arce, P. E. *J. Phys. Chem. C* **2007**, *111*, 16656.
(24) Zhu, Y.; Wang, C. *J. Phys. Chem. C* **2010**, *114*, 2830.
(25) Montella, C. *J. Electroanal. Chem.* **2002**, *518*, 61.
(26) Srinivasan, V.; Newman, J. *Electrochem. Solid-State Lett.* **2006**, *9*, A110.
(27) Yamada, A.; Chung, S. C. *J. Electrochem. Soc.* **2004**, *151*, A1352.
(28) Gabrisch, H.; Wilcox, J.; Doeff, M. M. *Electrochem. Solid-State Lett.* **2008**, *11*, A25.
(29) Striebel, K.; Shim, J.; Srinivasan, V.; Newman, J. *J. Electrochem. Soc.* **2005**, *152*, A664.
(30) Whittingham, M. S.; Song, Y.; Lutta, S.; Zavalij, P. Y.; Chernova, N. A. *J. Mater. Chem.* **2005**, *15*, 3362.
(31) Xu, J.; Chen, G.; Li, X. *Mater. Chem. Phys.* **2009**, *118*, 9.
(32) Xu, J.; Chen, G. *Electrochem. Solid-State. Lett.* **2009**, *12*, H399.

JP109954Y